PHOTONICS Research

Tapering-induced enhancement of light extraction efficiency of nanowire deep ultraviolet LED by theoretical simulations

Ronghui Lin,[1] Sergio Valdes Galan,[1] Haiding Sun,[1] Yangrui Hu,[1] Mohd Sharizal Alias,[2] Bilal Janjua,[2] Tien Khee Ng,[2] Boon S. Ooi,[2] and Xiaohang Li[1,*]

[1]Advanced Semiconductor Laboratory, King Abdullah University of Science and Technology (KAUST), Thuwal 23955-6900, Saudi Arabia
[2]Photonics Laboratory, King Abdullah University of Science and Technology (KAUST), Thuwal 23955-6900, Saudi Arabia
*Corresponding author: xiaohang.li@kaust.edu.sa

Received 18 December 2017; revised 19 February 2018; accepted 8 March 2018; posted 8 March 2018 (Doc. ID 315785); published 23 April 2018

A nanowire (NW) structure provides an alternative scheme for deep ultraviolet light emitting diodes (DUV-LEDs) that promises high material quality and better light extraction efficiency (LEE). In this report, we investigate the influence of the tapering angle of closely packed AlGaN NWs, which is found to exist naturally in molecular beam epitaxy (MBE) grown NW structures, on the LEE of NW DUV-LEDs. It is observed that, by having a small tapering angle, the vertical extraction is greatly enhanced for both transverse magnetic (TM) and transverse electric (TE) polarizations. Most notably, the vertical extraction of TM emission increased from 4.8% to 24.3%, which makes the LEE reasonably large to achieve high-performance DUV-LEDs. This is because the breaking of symmetry in the vertical direction changes the propagation of the light significantly to allow more coupling into radiation modes. Finally, we introduce errors to the NW positions to show the advantages of the tapered NW structures can be projected to random closely packed NW arrays. The results obtained in this paper can provide guidelines for designing efficient NW DUV-LEDs.

OCIS codes: (230.3670) Light-emitting diodes; (250.5590) Quantum-well, -wire and -dot devices.

https://doi.org/10.1364/PRJ.6.000457

1. INTRODUCTION

There is growing demand for mercury-free, environmentally friendly, compact deep ultraviolet light emitting diodes (DUV-LEDs) for applications such as disinfection [1], sensing [2], and polymer curing [3]. Currently, however, high-performance DUV-LEDs remain scarce. The external quantum efficiency (EQE) drops drastically with the wavelength, and most of the reported EQE is below 10% in the DUV region [4]. Apart from the poor crystalline quality and inefficient p-doping, another contributor to the low efficiency of existing AlGaN-based planar DUV-LEDs is the poor light extraction efficiency (LEE). Two main reasons lead to the poor LEE. The first is the absorption of the metal and the p-Ga(Al)N [5,6] contact layer. The second reason is the confinement of light due to the large refractive index (RI) of the materials and the reabsorption thereafter. Only the light emitted at angles smaller than the critical angle of total internal reflection (TIR) can be extracted successfully; the rest of the light will be coupled to the guided mode due to the TIR at the semiconductor–air interface. The guided light will be reabsorbed by the multiple quantum well (MQW) and p-Ga(Al)N, with only a low percentage eventually emitting at the edge of the device. The problem is more severe for DUV-LEDs because of large absorption of p-Ga(Al)N in the DUV region and the fact that most of the light will emit to angles larger than the critical angle because of the increasing of TM polarization as the wavelength becomes shorter [7–9]. These factors limit the LEE to be lower than 10% in the DUV range [10].

Recently, dislocation-free AlGaN nanowires (NWs) have been grown onto dissimilar substrates and fabricated into LEDs operating in the DUV region [11–13]. An internal quantum efficiency (IQE) of 70%–80% and output power of >8 mW are reported; however, the EQE is limited by the LEE due to the dominance of TM polarized emission and the high filling ratio of the NWs [13]. One way to enhance the LEE is to take advantage of the TM emission by lateral extraction, which is demonstrated numerically in Refs. [10,14]. Another method is to enhance the vertical LEE by periodic NW array, which can be explained by photonic crystal (PhC) theory [15,16]. There are two scenarios where the LEE can be enhanced by NW arrays. (i) The first mechanism can be explained by Bragg's law of diffraction, which is formulated as $\beta_d = \beta_i + G$, where β_i is the incident k-vector, G is the reciprocal lattice vector of the PhC,

and β_d is diffracted k-vector. Due to the periodic nature of the PhC, the guided mode will be folded at the Brillouin zone boundaries. The resultant modes with $\beta_d < k_0$, where k_0 is the k-vector for free space propagation that defines the light line, become radiation modes [17]. (ii) By choosing the emission frequency to locate in the middle of the photonic bandgap, the in-plane propagation is inhibited, and all the light will be forced to propagate in the vertical direction, thus enhancing the LEE. However, according to Fermi's golden rule, the spontaneous emission rate is proportional to the local photon density of states [18]. Therefore, the spontaneous emission will be greatly inhibited when the frequency of the source is in the bandgap region [19], leading to overall poor performance of light emission devices. Thus, it is usually more favorable to use the first scheme to enhance the LEE of LEDs [20,21]. To achieve this, the reciprocal vector G has to be carefully designed to make sure the diffraction condition can be met for a maximum number of modes and angles to ensure the large LEE. Typically, the maximum LEE can be achieved when the filling ratio of the PhC is between 0.4 and 0.6 [17]. However, such a low filling ratio is unfavorable for NW devices because it restricts the volume of the active region and hence the overall optical power. Besides, a large filling ratio is necessary to facilitate contact metal deposition [22]. There have been few reports on how to achieve enhanced LEE when the filling ratio of the NWs is high. Moreover, nearly all the spontaneously molecular beam epitaxy (MBE) grown AlGaN NWs are in the shape of tapering cones [23,24]. Yet, previous simulations [10,11,14,25] are carried out under the assumption that the radius of the NWs remained the same along the growth direction. Few studies investigate the LEE based on tapered NWs, especially in the DUV region.

In this study, we investigate the effects of the small tapering angle of closely packed AlGaN NWs on the LEE by numerical methods. First, the optical behavior of these arrays is studied in the theoretical framework of PhCs. Then, the light extraction and the far-field radiation are calculated for both TM and TE polarizations for the different tapering angles. The electric field distribution and the Bloch mode profiles of the NW array are also calculated to explain the enhancement. We show in our simulation that LEE, especially for TM polarization, can be enhanced by introducing a tapering angle for closely packed NWs with no structural optimization. Finally, some variations of the NW positions are added to break the periodicity to evaluate the effect of the random positions of NWs on the LEE.

2. SIMULATION SETUP

The structure of the NW array, as shown in Figs. 1(a) and 1(b), is composed of a hexagonal array of 121 NWs on a Si substrate. The design of the NW epilayers is based on our previous publication but is modified to make the emission wavelength around 260 nm [26]. Each NW consists of 5 nm p++-GaN, 15 nm p-GaN, 100 nm p-$Al_{0.65}Ga_{0.35}N$, 10 nm p-$Al_{0.85}Ga_{0.15}N$, 100 nm $Al_{0.65}Ga_{0.35}N/Al_{0.80}Ga_{0.20}N$ MQW active region, 200 nm n-$Al_{0.65}Ga_{0.35}N$, and 10 nm n-GaN layers. The RI and absorption coefficients of each layer are shown in Fig. 1(c), and specifically, the RI of the AlGaN layers are from our ellipsometry measurements, whereas the RI of GaN and Si are from Refs. [27,28]. The NW spacing and size are based on an

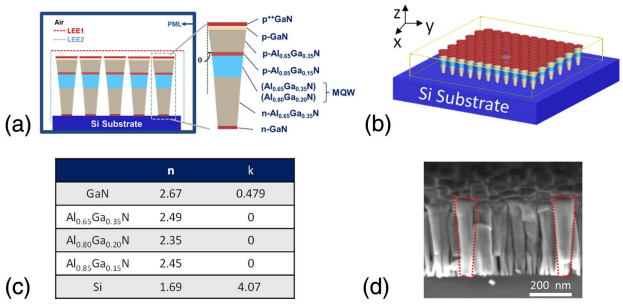

	n	k
GaN	2.67	0.479
$Al_{0.65}Ga_{0.35}N$	2.49	0
$Al_{0.80}Ga_{0.20}N$	2.35	0
$Al_{0.85}Ga_{0.15}N$	2.45	0
Si	1.69	4.07

Fig. 1. (a) Simulated NW DUV-LED structure. (b) 3D schematic of the NW array composed of a hexagonal periodic structure of 121 NWs. (c) RI of GaN, AlGaN, and silicon substrate. (d) Cross-sectional scanning electron microscope image of MBE-grown NWs [22].

experimental grown structure, as shown in Fig. 1(d), but the composition and thickness of the epilayers are slightly modified in order to control the emission wavelength. The light propagation and absorption are calculated using the 3D-FDTD (finite-difference time-domain) simulation. In the simulation, the height, top diameter, and pitch of the NWs are fixed to 440, 120, and 125 nm, respectively, while the tapering angle (θ) of the NWs is changed from 0° to 5.25° because 5.25° is approximately the largest tapering angle we observe in our experimental work as well as in previous publications [13,24,29]. Moreover, further increment of the tapering angle will result in the NWs to overlapping with each other, which gives us unfair comparison with the smaller tapering angle condition when the NWs are not coalesced. The tapering angles of the NW have been shown to be controllable by carefully tuning the growing parameters [30–32]. As shown in Fig. 1(b), an electric dipole source is positioned at the center of the NW array in the middle of the MQW active region [10]. In this study, we examined two optical polarizations: TE and TM, which correspond to the electric field direction perpendicular and parallel to the NW c-axis, respectively. The results of TE polarization were obtained by averaging the results from two different in-plane dipole directions. Three parameters, LEE, LEE1, and LEE2, are introduced to characterize the light extraction. LEE1 corresponds to vertical extraction, which is calculated as the ratio of the extracted power from the NW top surface to the total emitted power of the electric dipole. And LEE2 corresponds to the side extraction, which is calculated as the ratio of the emitted power from lateral sides of the NW array to the total power emitted by the electric dipole. The total LEE is calculated as the sum of LEE1 and LEE2. The arrangement of LEE1 and LEE2 is shown in Fig. 1(a).

3. RESULTS

The photonic band structures of the NW array are calculated using the MIT photonic-bands (MPB), which is an open source, three-dimensional eigensolver [33]. The photonic band structures along high symmetrical points Γ-M-K-Γ for $\theta = 0°$ and 5.25° are plotted in Fig. 2. The blue line, called the light line, separates the band diagram into two areas. The gray area above the light line corresponds to the continuum of radiation modes, while the modes below the light line are guided modes that are confined within the NW array. The guided modes

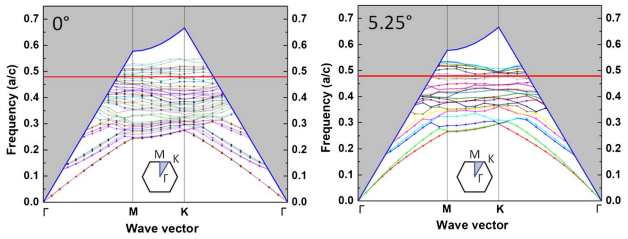

Fig. 2. Comparison of the band structures of NW arrays with $\theta = 0°$ and 5.25°. Horizontal red lines indicate the frequency of concern.

can be categorized as even and odd modes with respect to the symmetry along the vertical direction if no substrate is considered. However, because the existence of the substrate breaks the symmetry along the vertical direction, such categorization is no longer valid. For both 0° and 5.25° NW structures, no complete photonic bandgap is observed due to the close-packing nature of the NWs. The red line, which represents the frequency of concern in this paper, lies at a location with a large number of guided modes. The lack of a bandgap indicates the NW arrays are operated in the diffraction regime, as mentioned earlier. However, the large number of guided modes greatly reduced the effect of diffraction. The band structure for $\theta = 0°$ is denser than that for $\theta = 5.25°$, indicating the existence of more guided modes.

Figure 3 plots the LEE for both TE and TM polarizations as a function of θ ranging from 0° to 5.25°. For the TE polarized emission, as shown in Fig. 3(a), both the LEE and LEE1 increase in a fluctuated manner due to the strong and weak coupling to resonance modes in the NW structure. LEE1 is always higher than LEE2, which is reasonable because the TE emission travels largely in the vertical direction. At 5° tapering angle, both LEE and LEE1 reach their maximum value of 41.9% and 38.2%, respectively. In contrast, at 0° tapering angle, the values of LEE and LEE1 are 29.1% and 20.8%, respectively. The vertical extraction nearly doubles. For the TM polarized emission, as shown in Fig. 3(b), we also see a fluctuated increase in both LEE and LEE1. At 0° angle, the LEE and LEE1 are 20.9% and 4.8%, which increase to 38.4% and 24.3% at 5.25°, respectively. The LEE increases by nearly 200% and LEE1 by nearly 500%. Although LEE1 is not always dominant over LEE2 at all angles for TM polarization, we do observe higher LEE1 at certain angles. The increase of vertical light extraction is consistent for both TE and TM polarizations. The side extraction LEE2 corresponds to the guided light that is extracted from the lateral direction. However, due to the larger size of the array in the actual situation, a large portion of LEE2 will be absorbed by MQW and p-GaN before reaching the edge. Moreover, as the array size gets larger, the area-to-peripheral ratio decreases, and the area of the top surface increases more rapidly than the side surface area; thus, it is more favorable to have higher extraction efficiency at the top surface (LEE1). We note that the dramatic enhancement of LEE1 from 4.8% to 24.3% for TM polarization is particularly profound because a larger portion of the DUV emission is TM polarized [34].

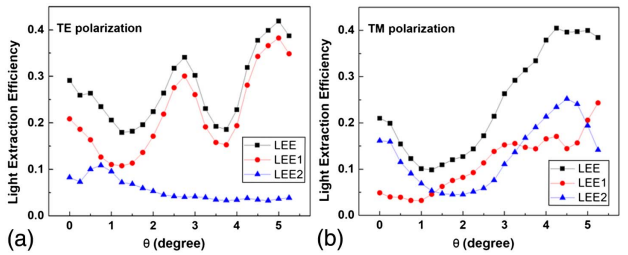

Fig. 3. LEE versus tapering angle θ for (a) TE polarized emission and (b) TM polarized emission.

To gain complete understanding of the light extraction in the NW structure, Fig. 4 exemplarily shows a comparison of the electric field intensity distribution for the investigated NW structure with no tapering angle and the NW structure with a tapering angle of 5.25° in cross-sectional and top views. For both TE and TM polarizations in un-tapered NWs, a large portion of the field is confined to the guided mode of the PhC [35], with little radiation at the top surface of the NWs.

Because of the narrow spacing (5 nm) between the NWs, the PhC effect has become weak [36]; thus, the TIR cannot be effectively diffracted to the radiation mode [17]. However, as the tapering angle increases to 5.25°, the electric field intensity at the top surface is greatly enhanced, as shown in Fig. 4(a). The light will be diffracted to the vertical direction due to the gradient of effective RI in the tapered NW array. Significant differences also exist in electric field distribution within each individual NW for 0° and 5.25° tapering angles.

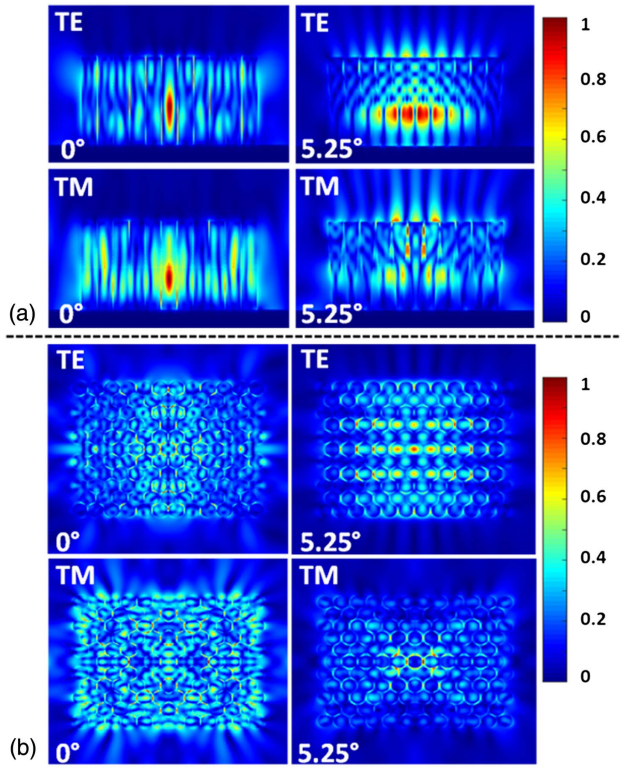

Fig. 4. Electric field intensity distribution for (a) cross-sectional view and (b) top view for TE and TM modes in a conventional cylindrical structure ($\theta = 0°$) and a structure with tapering angle ($\theta = 5.25°$).

From the side view shown in Fig. 4(a), we observe that more vertical nodes exist in the 5.25° NWs, while in the top view shown in Fig. 4(b), more azimuth nodes exist in the NW with the 0° tapering angle. This is because the reduced diameter at the bottom of the NWs is unable to support high azimuth modes.

To show how the tapering angle influences the far field radiation of the NW array, the normalized angular intensity distributions of 0°, 2.5°, and 5.25° are obtained by propagating the field at the top monitor to the far-field and plotted in Fig. 5. The intensity distribution exhibits hexagonal symmetry due to the hexagonal nature of our NW array [37]. At 0° angle, the far-field intensity is more concentrated, but, as the angle increases, not only the far-field intensity increases, the field is also distributed in a larger angular direction. This trend is similar for both TE and TM emissions as shown in Figs. 6(a) and 6(b), respectively.

To gain more insight into how the geometry influences the light propagation, some of the Bloch mode profiles at the K point of the band diagrams are plotted in Fig. 6. Because of the hexagonal symmetry of the NWs, only a single NW is simulated in the unit cell when calculating the mode profiles. To show a clear comparison, modes with similar node numbers and profiles are shown in the figure. As can be seen in Fig. 6, although the substrate introduced a small perturbation to the structure, the mode shapes are more or less symmetrical in the vertical direction for an NW array with 0° tapering angle. However, as the tapering angle is introduced, the mode profile is pushed and squeezed to the top of the NW despite the same number of nodes for tapered structure and cylindrical structure. The broken symmetry in the vertical direction disrupts the in-plane Bloch mode propagation of the light. Intuitively, the tapering walls of NWs add another TIR interface that guides light toward the top. It has been reported that PhC waveguides based on cone structures suffer from more propagation losses due to out-of-plane structural asymmetries [38]. However, this characteristic works to our advantage in the light extraction of LED. Another observation from Fig. 6 is that a large portion of the field exists in the air at the bottom of the tapered NW. This is because the small diameter at the bottom is not enough to support guide modes. Hence, the modes become leaky at the bottom, which increase the coupling to radiation modes; therefore, we can see enhanced field distribution at the top and side of the NW in all the mode profiles shown in Fig. 6, which also explains the enhanced LEE.

In the actual devices grown by MBE, the positions of the NWs are usually not strictly periodic [11,23]. To project our results to the actual device, we introduce positional errors to the periodic NW arrays to study their influence on the LEE. The errors are introduced by adding random noise to the x and y coordinates of each NW. Because the pitch of the periodic NWs is 5 nm, the noises for both x and y coordinates are generated with standard deviation values ranging from 1 to 5 nm. For each standard deviation value of the positional error, five simulations are carried out; the average and the standard errors of the LEE are plotted in Fig. 7. Generally, we see that the randomization of the position does impose some fluctuations on the LEE due to the introduction of localization and random scattering effect [24,39]. The LEE fluctuates from 38.7% to 41.4% for TE and from 38.4% to 33.1% for TM. Similarly, LEE1 fluctuates from 34.8% to 36.1% for TE and from 24.3% to 17.1% for TM. Despite this, we observe higher LEE1 than LEE2 consistently at 5.25° for both TE and TM emissions. Moreover, by the comparison between the tapering angles of 5.25° to 0°, we notice a higher LEE and LEE1 for both TE

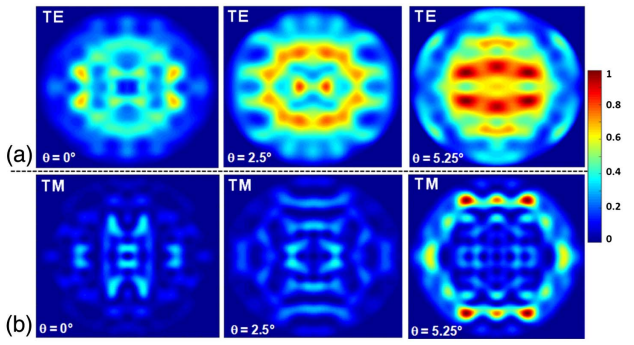

Fig. 5. Far-field intensity distribution of (a) TE polarization mode and (b) TM polarization mode for $\theta = 0°$, 2.5°, and 5.25°.

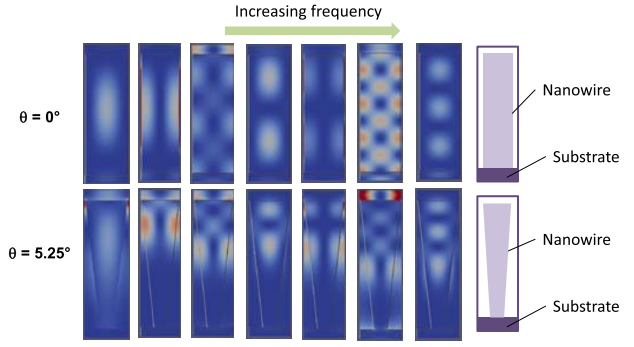

Fig. 6. Comparison of Bloch mode profiles of NW array with the tapering angles of 0° and 5.25°.

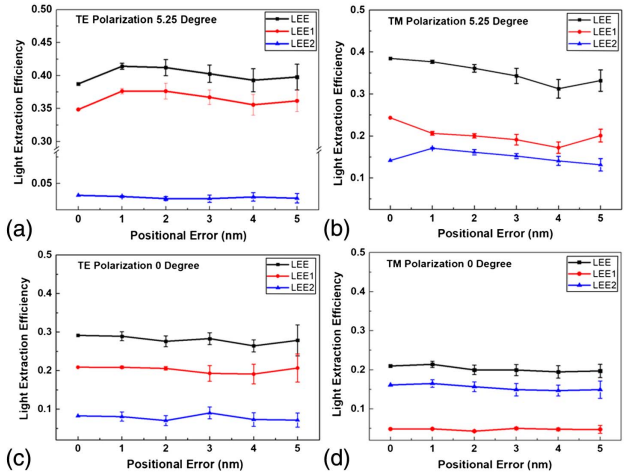

Fig. 7. Influence of the positional error on the LEE of (a) 5.25° tapering angle TE polarized emission, (b) 5.25° tapering angle TM polarized emission, (c) 0° tapering angle TE polarized emission, and (d) 0° tapering angle TM polarized emission.

and TM polarizations with 5.25° tapering angle, which indicates that the advantages of the tapering angle can also be projected to closely packed randomly distributed NWs. This is because only small perturbations can be added to the positions of the NWs under the closely packed condition.

4. CONCLUSIONS

The LEE of AlGaN-based NW LEDs emitting at DUV wavelengths has been simulated with a tapered NW shape. We have shown that the total LEE increased from 29.1% to 41.9% for TE polarization and from 20.9% to 38.4% for TM polarization by adding a tapering angle of 5.25°. Most notably, the vertical extraction of TM emission increased from 4.8% to 24.3%. The big enhancement for TM is significant because the emission for DUV-LEDs is predominantly TM polarized, which is extremely difficult to be extracted. The Bloch mode study of tapered and untapered NWs shows that the mode shapes of the tapered NWs are leaky and promote diffraction toward the top of the NWs, allowing more radiation into the free space. Finally, we show that the advantage of a tapering angle can also be projected to randomly distributed NWs.

Funding. King Abdullah University of Science and Technology (KAUST) (KAUST Baseline Fund BAS/1/1614-01-01, KAUST Baseline Fund BAS/1/1664-01-01, KAUST Equipment Fund BAS/1/1664-01-07); National Natural Science Foundation of China (NSFC) (61774065).

Acknowledgment. The authors would like to acknowledge the support of the KAUST Baseline Fund and KAUST Equipment Fund. Xiaohang Li also appreciates the support of the National Natural Science Foundation of China.

REFERENCES

1. M. A. Wurtele, T. Kolbe, M. Lipsz, A. Kulberg, M. Weyers, M. Kneissl, and M. Jekel, "Application of GaN-based ultraviolet-C light emitting diodes—UV LEDs—for water disinfection," Water Res. **45**, 1481–1489 (2011).
2. A. J. Hopkins, J. L. Cooper, L. T. M. Profeta, and A. R. Ford, "Portable deep-ultraviolet (DUV) Raman for standoff detection," Appl. Spectrosc. **70**, 861–873 (2016).
3. S. J. Choi, J. H. Kim, and H. H. Lee, "Deep-UV curing of poly(4-vinyl phenol) gate dielectric for hysteresis-free organic thin-film transistors," IEEE Electron Device Lett. **30**, 454–456 (2009).
4. J. Rass, T. Kolbe, N. L. Ploch, T. Wernicke, F. Mehnke, C. Kuhn, J. Enslin, M. Guttmann, C. Reich, A. Mogilatenko, J. Glaab, C. Stoelmacker, M. Lapeyrade, S. Einfeldt, M. Weyers, and M. Kneissl, "High power UV-B LEDs with long lifetime," Proc. SPIE **9363**, 93631K (2015).
5. H. Y. Ryu, I. G. Choi, H. S. Choi, and J. I. Shim, "Investigation of light extraction efficiency in AlGaN deep-ultraviolet light-emitting diodes," Appl. Phys. Express **6**, 062101 (2013).
6. H. Hirayama, T. Takano, J. Sakai, T. Mino, K. Tsubaki, N. Maeda, M. Jo, Y. Kanazawa, I. Ohshima, T. Matsumoto, and N. Kamata, "Realization of over 10% EQE AlGaN deep-UV LED by using transparent p-AlGaN contact layer," in *2016 International Semiconductor Laser Conference* (IEEE, 2016), pp. 1–2.
7. R. G. Banal, M. Funato, and Y. Kawakami, "Optical anisotropy in [0001]-oriented $Al_xGa_{1-x}N$/AlN quantum wells ($x > 0.69$)," Phys. Rev. B **79**, 121308 (2009).
8. X. J. Chen, C. Ji, Y. Xiang, X. N. Kang, B. Shen, and T. J. Yu, "Angular distribution of polarized light and its effect on light extraction efficiency in AlGaN deep-ultraviolet light-emitting diodes," Opt. Express **24**, A935–A942 (2016).
9. J. Zhang, H. P. Zhao, and N. Tansu, "Effect of crystal-field split-off hole and heavy-hole bands crossover on gain characteristics of high Al-content AlGaN quantum well lasers," Appl. Phys. Lett. **97**, 111105 (2010).
10. M. Djavid and Z. T. Mi, "Enhancing the light extraction efficiency of AlGaN deep ultraviolet light emitting diodes by using nanowire structures," Appl. Phys. Lett. **108**, 051102 (2016).
11. S. Zhao, S. M. Sadaf, S. Vanka, Y. Wang, R. Rashid, and Z. Mi, "Sub-milliwatt AlGaN nanowire tunnel junction deep ultraviolet light emitting diodes on silicon operating at 242 nm," Appl. Phys. Lett. **109**, 201106 (2016).
12. T. F. Kent, S. D. Carnevale, A. T. M. Sarwar, P. J. Phillips, R. F. Klie, and R. C. Myers, "Deep ultraviolet emitting polarization induced nanowire light emitting diodes with $Al_xGa_{1-x}N$ active regions," Nanotechnology **25**, 455201 (2014).
13. S. M. Sadaf, S. Zhao, Y. Wu, Y. H. Ra, X. Liu, S. Vanka, and Z. Mi, "An AlGaN core-shell tunnel junction nanowire light-emitting diode operating in the ultraviolet-C band," Nano Lett. **17**, 1212–1218 (2017).
14. M. Djavid, D. D. Choudhary, M. Rajan Philip, T. H. Q. Bui, O. Akinnuoye, T. T. Pham, and H. P. T. Nguyen, "Effects of optical absorption in deep ultraviolet nanowire light-emitting diodes," Photon. Nanostr. Fundam. Appl. **28**, 106–110 (2018).
15. J. J. Wierer, A. David, and M. M. Megens, "III-nitride photonic-crystal light-emitting diodes with high extraction efficiency," Nat. Photonics **3**, 163–169 (2009).
16. A. A. Erchak, D. J. Ripin, S. Fan, P. Rakich, J. D. Joannopoulos, E. P. Ippen, G. S. Petrich, and L. A. Kolodziejski, "Enhanced coupling to vertical radiation using a two-dimensional photonic crystal in a semiconductor light-emitting diode," Appl. Phys. Lett. **78**, 563–565 (2001).
17. C. Wiesmann, K. Bergenek, N. Linder, and U. T. Schwarz, "Photonic crystal LEDs—designing light extraction," Laser Photon. Rev. **3**, 262–286 (2009).
18. E. M. Purcell, "Spontaneous emission probabilities at radio frequencies," Phys. Rev. **69**, 681 (1946).
19. M. Fujita, S. Takahashi, Y. Tanaka, T. Asano, and S. Noda, "Simultaneous inhibition and redistribution of spontaneous light emission in photonic crystals," Science **308**, 1296–1298 (2005).
20. H. D. Sun, A. Piquette, M. Raukas, and T. D. Moustakas, "Enhancement of yellow light extraction efficiency of $Y_3Al_5O_{12}:Ce^{3+}$ ceramic converters using a 2-D TiO_2 hexagonal-lattice nanocylinder photonic crystal layer," IEEE Photon. J. **8**, 4500310 (2016).
21. A. David, T. Fujii, R. Sharma, K. McGroddy, S. Nakamura, S. P. DenBaars, E. L. Hu, C. Weisbuch, and H. Benisty, "Photonic-crystal GaN light-emitting diodes with tailored guided modes distribution," Appl. Phys. Lett. **88**, 061124 (2006).
22. B. Janjua, H. Sun, C. Zhao, D. H. Anjum, F. Wu, A. A. Alhamoud, X. Li, A. M. Albadri, A. Y. Alyamani, M. M. El-Desouki, T. K. Ng, and B. S. Ooi, "Self-planarized quantum-disks-in-nanowires ultraviolet-B emitters utilizing pendeo-epitaxy," Nanoscale **9**, 7805–7813 (2017).
23. S. Zhao, S. Y. Woo, S. M. Sadaf, Y. Wu, A. Pofelski, D. A. Laleyan, R. T. Rashid, Y. Wang, G. A. Botton, and Z. Mi, "Molecular beam epitaxy growth of Al-rich AlGaN nanowires for deep ultraviolet optoelectronics," APL Mater. **4**, 086115 (2016).
24. K. H. Li, X. Liu, Q. Wang, S. Zhao, and Z. Mi, "Ultralow-threshold electrically injected AlGaN nanowire ultraviolet lasers on Si operating at low temperature," Nat. Nanotechnol. **10**, 140–144 (2015).
25. Q. Y. Yue, K. Li, F. M. Kong, J. Zhao, and W. Li, "Analysis on the light extraction efficiency of GaN-based nanowires light-emitting diodes," IEEE J. Quantum Electron. **49**, 697–704 (2013).
26. B. Janjua, H. D. Sun, C. Zhao, D. H. Anjum, D. Priante, A. A. Alhamoud, F. Wu, X. H. Li, A. M. Albadri, A. Y. Alyamani, M. M. El-Desouki, T. K. Ng, and B. S. Ooi, "Droop-free $Al_xGa_{1-x}N/Al_yGa_{1-y}N$ quantum-disks-in-nanowires ultraviolet LED emitting at 337 nm on metal/silicon substrates," Opt. Express **25**, 1381–1390 (2017).
27. D. E. Aspnes and A. A. Studna, "Dielectric functions and optical-parameters of Si, Ge, GaP, GaAs, GaSb, InP, InAs, and InSb from 1.5 to 6.0 eV," Phys. Rev. B **27**, 985–1009 (1983).

28. S. Adachi, *Optical Constants of Crystalline and Amorphous Semiconductors: Numerical Data and Graphical Information* (Kluwer Academic Publishers, 1999).
29. S. Zhao, X. Liu, S. Y. Woo, J. Kang, G. A. Botton, and Z. Mi, "An electrically injected AlGaN nanowire laser operating in the ultraviolet-C band," Appl. Phys. Lett. **107**, 043101 (2015).
30. S. D. Carnevale, J. Yang, P. J. Phillips, M. J. Mills, and R. C. Myers, "Three-dimensional GaN/AlN nanowire heterostructures by separating nucleation and growth processes," Nano Lett. **11**, 866–871 (2011).
31. S. Fernandez-Garrido, X. Kong, T. Gotschke, R. Calarco, L. Geelhaar, A. Trampert, and O. Brandt, "Spontaneous nucleation and growth of GaN nanowires: the fundamental role of crystal polarity," Nano Lett. **12**, 6119–6125 (2012).
32. A. Pierret, C. Bougerol, S. Murcia-Mascaros, A. Cros, H. Renevier, B. Gayral, and B. Daudin, "Growth, structural and optical properties of AlGaN nanowires in the whole composition range," Nanotechnology **24**, 115704 (2013).
33. S. G. Johnson and J. D. Joannopoulos, "Block-iterative frequency-domain methods for Maxwell's equations in a planewave basis," Opt. Express **8**, 173–190 (2001).
34. T. Kolbe, A. Knauer, C. Chua, Z. H. Yang, S. Einfeldt, P. Vogt, N. M. Johnson, M. Weyers, and M. Kneissl, "Optical polarization characteristics of ultraviolet (In)(Al)GaN multiple quantum well light emitting diodes," Appl. Phys. Lett. **97**, 171105 (2010).
35. S. G. Johnson, S. H. Fan, P. R. Villeneuve, J. D. Joannopoulos, and L. A. Kolodziejski, "Guided modes in photonic crystal slabs," Phys. Rev. B **60**, 5751–5758 (1999).
36. D. R. Solli and J. M. Hickmann, "Study of the properties of 2D photonic crystal structures as a function of the air-filling fraction and refractive index contrast," Opt. Mater. **33**, 523–526 (2011).
37. P. F. Zhu and N. Tansu, "Effect of packing density and packing geometry on light extraction of III-nitride light-emitting diodes with microsphere arrays," Photon. Res. **3**, 184–191 (2015).
38. Y. Tanaka, T. Asano, Y. Akahane, B. S. Song, and S. Noda, "Theoretical investigation of a two-dimensional photonic crystal slab with truncated cone air holes," Appl. Phys. Lett. **82**, 1661–1663 (2003).
39. J. W. Kim, J. H. Jang, M. C. Oh, J. W. Shin, D. H. Cho, J. H. Moon, and J. I. Lee, "FDTD analysis of the light extraction efficiency of OLEDs with a random scattering layer," Opt. Express **22**, 498–507 (2014).